INTERNATIONAL JOURNAL OF REFRIGERATION 73 (2017) 99–110

Available online at www.sciencedirect.com

ScienceDirect

journal homepage: www.elsevier.com/locate/ijrefrig

An experimental and numerical study of refrigerator heat leakage at the gasket region

Feng Gao [a], *Shervin Shoai Naini* [b], *John Wagner* [b], *Richard Miller* [b,*]

[a] *Department of Mechanical Engineering, New Jersey Institute of Technology, Newark, NJ 07102-1824, USA*
[b] *Department of Mechanical Engineering, Clemson University, Clemson, SC 29634-0921, USA*

ARTICLE INFO

Article history:
Received 27 May 2016
Received in revised form 29 July 2016
Accepted 2 September 2016
Available online 7 September 2016

Keywords:
Refrigerators
Heat leakage
Computational fluid dynamics
Reverse heat load method
Experimental testing

ABSTRACT

A combined experimental and computational approach was developed to measure the heat leakage through the refrigerator gasket region. The experiment was carried out by measuring the heat flux through the door gasket by Reverse Heat Load Method (RHLM). The experimental point measurements lie near to the continuous curve from Computational Fluid Dynamics (CFD) simulation, which makes it reasonable to provide a dimensionless shape profile by CFD to fill in the missing information between experimental measurement points in order to provide the actual effective heat leakage. The average effective heat leakage on the door gasket surface is determined as $0.2\ W\ m^{-1}\ K^{-1}$ comprising 17% and 14% heat leakage of the total load in the fresh-food and freezer compartments, respectively. The electric fan and the hot pipe along the perimeter of the door contribute to an increase of 20% and 10% in the effective heat leakage on the door surface of the freezer, respectively.

Étude expérimentale et numérique portant sur la fuite thermique constatée dans un réfrigérateur au niveau du joint

Mots clés : Réfrigérateurs ; Fuite thermique ; Mécanique des fluides numérique ; Méthode inverse de la charge thermique ; Essais expérimentaux

1. Introduction

Refrigerators are one of the most widely used consumer appliances and are required to meet strict energy efficiency ratings. Investigating the heat leakage of refrigerators is of great practical meaning, especially concerning the reduction of unnecessary energy consumption. Although many researchers (Brent et al., 1995; Gupta et al., 2007; Xie and Bansal, 2000) have studied the influence of multiple variables on the energy consumption of refrigerators, little attention has been focused on the door gasket heat leakage of refrigerators. The heat

* *Corresponding author.* Department of Mechanical Engineering, Clemson University, 210 Engineering Innovation Building, Clemson, SC 29634-0921, USA. Fax: +1 864 656 4435.
E-mail address: rm@clemson.edu (R. Miller).
http://dx.doi.org/10.1016/j.ijrefrig.2016.09.002

Nomenclature

Symbols

A-F	heat flux sensors along gasket
c	specific heat of capacity [J kg^{-1} K^{-1}]
Cu	empirical constant
Exp_n	experimental point measurement of the heat flux sensors [W m^{-2} (n = 1, 2, 3. . .6)]
f_n	CFD measurement of the heat flux corresponding to the experimental measurement points [W m^{-2} (n = 1, 2, 3. . .6)]
F	blending function
g	gravity [m s^{-2}]
H	heat load [W]
h	effective heat leakage [W m^{-1} K^{-1}]
I	turbulence intensity
K	thermal conductivity [W m^{-1} K^{-1}]
L	gasket surface length [m]
l	turbulent length scale [m]
p	pressure [Pa]
P	power [W]
q	heat flux [W m^{-2}]
Q	heat leakage at the gasket region [W]
Ra	Raleigh number
S	invariant of strain rate [s^{-1}]
s	coordinate along the outside of the gasket surface [m]
s''	coordinate along the inside of the gasket surface [m]
T	temperature of the flow inside the compartment [K]
ΔT	temperature difference between the ambient environment and the refrigerator compartment [K]
t	time [s]
k	turbulence kinetic energy [m^2 s^{-2}]
u	velocity of flow inside the compartment [m s^{-1}]

Greek symbols

α	correction factor in Least Mean Square Error analysis
β	thermal expansion coefficient
β^*	model constant
η	percentage of heat leakage at the gasket region accounted by total energy
μ	turbulence eddy diffusivity [m^2 s^{-1}]
ρ	density [kg m^{-3}]
σ'	model constant
ω	turbulence dissipation rate [s^{-1}]

Subscripts

cmp	compressor
ef	electric fan
f	freezer
g	gasket
int	initial
m	insulation material
n	indication of number heat flux sensors (n = 1, 2. . .6)
o	operating
rhl	reverse heat load
rms	root mean square
t	turbulence

leakage at the door gasket contributes to a significant percentage of the energy consumption of the refrigerator and freezer. Most related research (Boughton et al., 1996; Flynn et al., 1992; Ghassemi and Shapiro, 1991; Hasanuzzaman et al., 2009; Hessami and Hilligweg, 2003; Tao and Sun, 2001) indicates that the heat leakage at the door gasket accounts for 10%–30% of the total energy consumption depending on the insulation material and refrigerator specifications. It is important for the gasket to conform to the contour of the refrigerator door surface and be compressible and flexible enough to overcome the geometrical tolerance (Bansal et al., 2011). The heat transfer at the gasket is further complicated by the non-uniform temperature distribution inside the refrigerator cabinet (Conceição António and Afonso, 2011; Fukuyo et al., 2003; Laguerre et al., 2007). For the purpose of reducing the energy consumption of the refrigerator, more attention should be focused on improving the efficiency of the gasket region of the refrigerator. One possible reason for the sparse available open literature on door gasket heat leakage is that the heat transfer at the gasket is largely dependent on the variations of the cabinet and door designs of different types of refrigerators. Furthermore, the difficulty of accurate measurement due to the complex curved surface of the refrigerator door is a challenge.

The most commonly used experimental method to investigate heat leakage is the Reverse Heat Load Method (RHLM) (Hessami and Hilligweg, 2003; Sim and Ha, 2011; Tao and Sun, 2001). RHLM is an experimental setup in which a heat source is placed inside the refrigerator which is generally put into a controlled temperature–humidity chamber. This method is based on the principle that the energy input to maintain steady state equates with the heat leakage of the refrigerator. However, challenges are exposed when measuring the heat transfer at the gasket region by RHLM. Firstly, only a limited number of thermocouples are used for point measurements while the heat transfer at the door gasket region varies due to the complex curve shape and different thermal properties of insulation materials, therefore, it is not accurate to estimate the total heat leakage at the gasket region based on a few point measurements. Secondly, the RHLM does not account for the effect of the compressor and the operation of the electric fan inside the chamber of the freezer compartment in real working condition of refrigerator. Furthermore, the hot loop (e.g., the perimeter of the freezer section) generates extra heat to prevent dewing at the door gasket, which should be considered as it may contribute more heat leakage.

Computational Fluid Dynamics (CFD) is a prevalent numerical method to study the heat transfer at the door gasket. Sim and Ha (2011) show that a stagnant zone is formed at the gasket such that the air inside the refrigerator chamber cannot

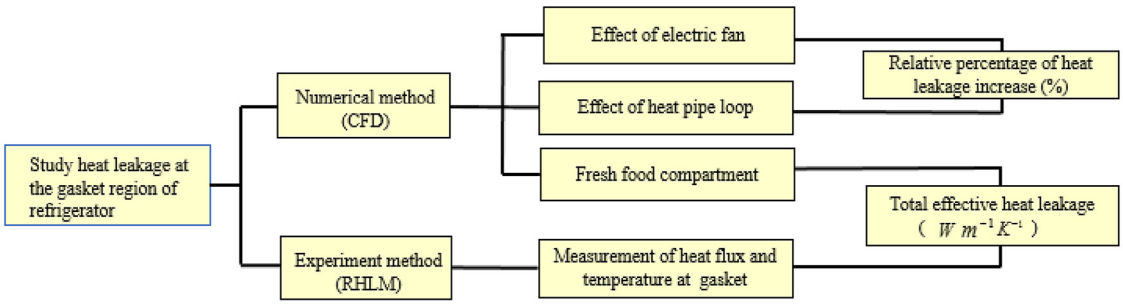

Fig. 1 – Heat leakage study; numerical and experimental activities diagram.

go through the gasket region completely. Huelsz et al. (2011) further evaluate the buoyancy effect of the air on the heat leakage at the door gasket region. In the above simulations, constant temperature (or temperature gradient) is implemented as the boundary condition. Although it can be appropriate to use constant temperature for the ambient environment as the environment is mostly at steady state, more attention needs to be paid on modeling the flow and temperature field inside the refrigerator and freezer compartment, especially the near wall region, as the shear flow near the wall region can significantly influence the heat leakage at the door gasket surface.

One popular method of modeling heat transfer for the HVAC system is Artificial Neural Network (ANN), which is independent of specific heat transfer equations and uses limited training data and computerizes by restoring the learning mechanism (Mohanraj et al., 2012). The reliability of ANN depends on the model architecture and the input of training and testing data (Mohanraj et al., 2015). Compared to ANN, CFD solves for partial differential equations basing on turbulent models. When properly modeled, CFD results can be provided as training and testing data for ANN (Conceição António and Afonso, 2011; Kumlutaş et al., 2012). Thus, one benefit of the present study is to provide a reliable database for establishing ANN models to provide gasket design and parameter modification assessment in the future.

In this paper, we combined RHLM with Computational Fluid Dynamics (CFD) to provide a robust method to evaluate the heat leakage at the gasket region of a domestic refrigerator. Both the (time averaged) interior and exterior temperatures are measured with thermocouples and the heat flux at specific points along the gasket surface is measured by heat flux sensors. Detailed Computational Fluid Dynamics (CFD) simulations were conducted to match the experimental conditions but using a two-dimensional slice and matching the exposed gasket section. Being two-dimensional, the CFD simulations are not meant to predict the actual heat transfer and temperature found in the experiment, but provides a "shape profile" of the heat flux leaving the gasket region along the gasket surfaces, on which the experimental heat flux sensors are placed. This shape profile was matched by a Least Mean Square Error (LMSE) analysis to the experimental data that essentially fills in the missing information between heat flux sensors. The intent and the focus of the present study are shown in Fig. 1.

2. Experimental study

The experiment was carried out based on a domestic refrigerator whose freezer compartment is 0.11 m^{-3} and fresh-food compartment is 0.39 m^{-3}. Fig. 2a shows the experimental apparatus, which is the concept designed to operate by placing a heat source within an inner box, then bringing the entire mass to a thermal steady state. The geometry and heat leakage complexity of real refrigerator cabinet are the major reasons for designing and building a simplified test cabinet concept for measuring the heat leakage through the gasket region (Fig. 2b). The experimental test cabinet is an insulated cubic box with a 216,000 cm^3 interior enclosure ($60\,cm \times 60\,cm \times 60\,cm$) which is designed to accept a matching set of adjoining refrigerator door and wall cuts placed inside the cavity. The door and walls are surrounded by a thick insulation material so that only the gasket region is exposed to the ambient environment. The "gasket region" is defined as the meeting of a 16 cm deep edge of the door section with a 15 cm section of the adjoining wall. A heat source is placed inside the center of the box to create a desired temperature difference between the interior and the ambient. It is directly wired to a power supplier placed out of the box (Fig. 2c). A data acquisition system, which is connected to a personal computer, is used to record the reading of thermocouples and heat flux sensors.

2.1. *Temperature measurements*

We used three different gaskets in Fig. 2d to perform experimental measurements. All measurements were carried out under steady state condition. The following steps were taken to confirm that the test cabinet reached steady state. Firstly, the primary data of inner air and ambient temperatures were recorded until they did not change with time. Then, the running averaged temperature was calculated as a function of time to determine how long averaging must be done to achieve converged experimental values, as shown in Fig. 3a. To quantify the deviation from the averaged values, the next step was to calculate the standard deviation from all data points after determining the average. Fig. 3b illustrates a running calculation of the standard deviation of a temperature signal versus time.

During the experiment, it was observed that heat flux linearly increases with the increase of temperature difference between the chamber and ambient environment, which

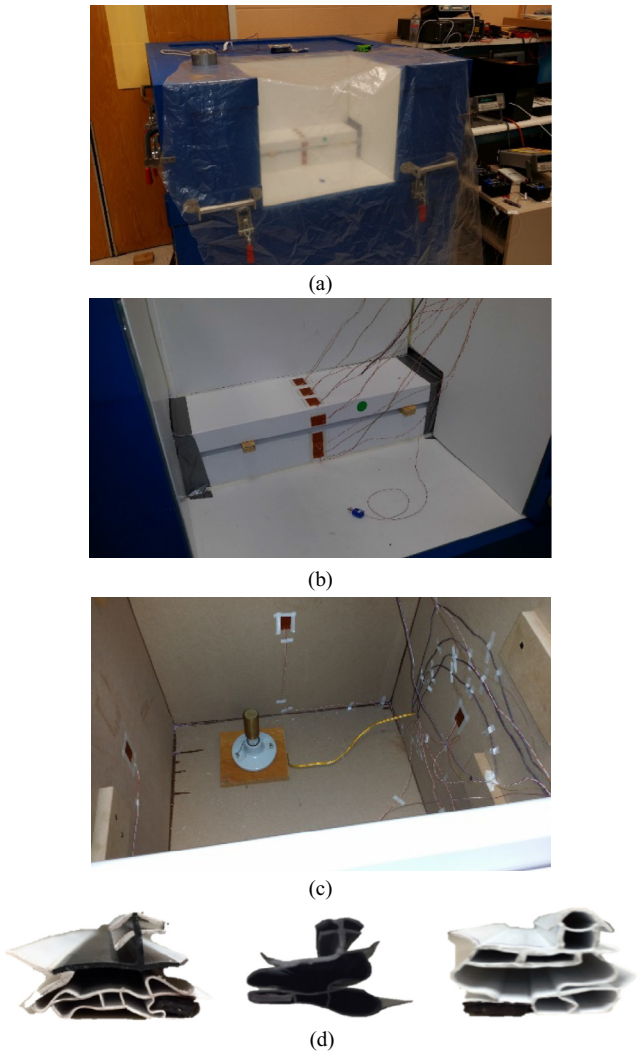

Fig. 2 – (a) Experimental test cabinet, (b) heat flux sensors positioned on the exposed portion of the gasket region, (c) inside of instrumented experimental apparatuses, and (d) photographs of the cross sections for gaskets 1 through 3.

indicates the linearity of the thermal property of the gasket material. Thus, it is appropriate to use RHLM as the final obtained effective gasket heat leakage is independent of temperature difference, which makes the measurement comparable to the effective heat leakage in real refrigerator operating performance. From a "cold" start, it was found that it takes approximately three days to reach steady state condition. The five experiments were run for three different gasket models and three different input heat loads. The temperature differences created across the gasket due to the applied heat load in each experiment are reported in Table 1.

2.2. *Heat flux measurements*

The heat flux sensor signals were treated in a similar manner. Both running average and standard deviations of heat flux data are calculated for all. Figs. 4 and 5 illustrate a typical (steady state) heat flux sensor instantaneous reading, running average, and running standard deviation, respectively. Based on the measurements, the heat leakage at the gasket region varies in a linear manner with respect to temperature difference by using RHLM.

All sensors were sampled at 0.5 Hz, which provides a sufficient time resolution of all signals while maintaining reasonable data file sizes for post processing of the averages and standard deviations. Final averages and standard deviations from all six heat flux sensors from all five experiments are provided in the Appendix.

Table 1 – Recorded temperature difference for three different gaskets with a single heat load (in which P_{rhl} is the reverse heat load implemented inside the compartment of the refrigerator by RHLM, ΔT is the temperature difference between the ambient environment and the measured steady state temperature of air inside the test cabinet).

Experiment no.	Gasket	P_{rhl} (W)	ΔT (K)
1	1 (original)	9.2	20.2
2		13.14	26.6
3		18.13	34.6
4	2 (black side-by-side)	13.14	25.2
5	3 (white)	13.14	25.6

2.3. *Repeatability of experiment measurement*

Repeatability of the experiments was also thoroughly investigated. Several of the experiments were repeated with more than a week between runs (Runs 1 and 2). Fig. 6 provides an example of two such data sets that were obtained for the conditions of the experiment with the white gasket (Experiment #5). Data are shown from two different runs of the same experiment performed, demonstrating the reproducibility of the results. The "error" bars are the standard deviation of the data used to calculate the average heat fluxes.

3. Numerical simulations

CFD simulation was carried out by using commercial software package ANSYS FLUENT®. The heat transfer mechanisms inside the freezer and refrigerator compartments are different, which in turn influence the heat transfer at the door gasket. As for the refrigerator compartment, natural convection is dominant as Ra is ranging from 10^8 to 10^9 (Laguerre et al., 2005). For the heat transfer inside the freezer compartment, forced convection is dominant when the electric fan (synchronized with the operation of the compressor) is in operation. The thermal properties related to the door gasket in the CFD simulation are listed in Table 2, in which ρ_m, c_m and K_m are the density, specific heat of capacity and thermal conductivity of the insulation materials, respectively. Fig. 7 shows a 2D geometry of the experimental test cabinet.

For the present work, it is assumed that the air inside the chamber of the refrigerator is incompressible. The Boussinesq equations are applied and heat dissipation is negligible (Huelsz

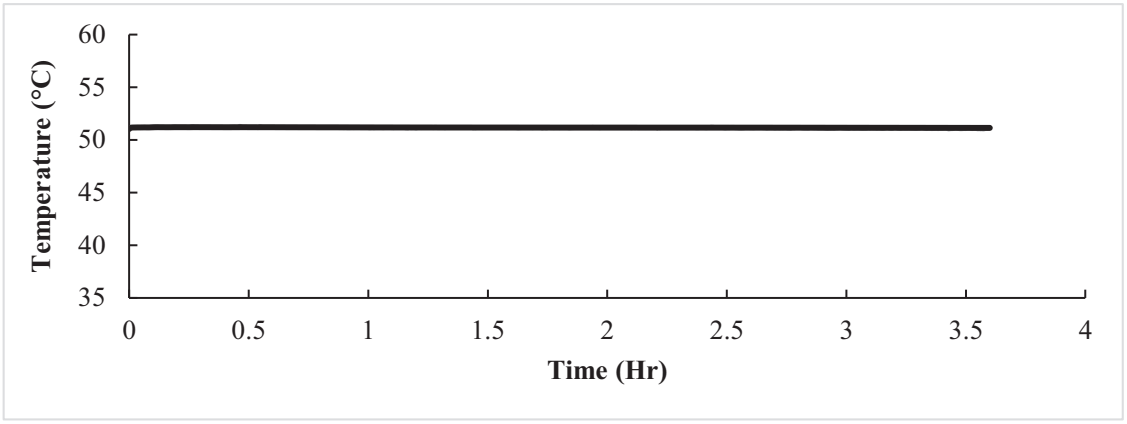

(a)

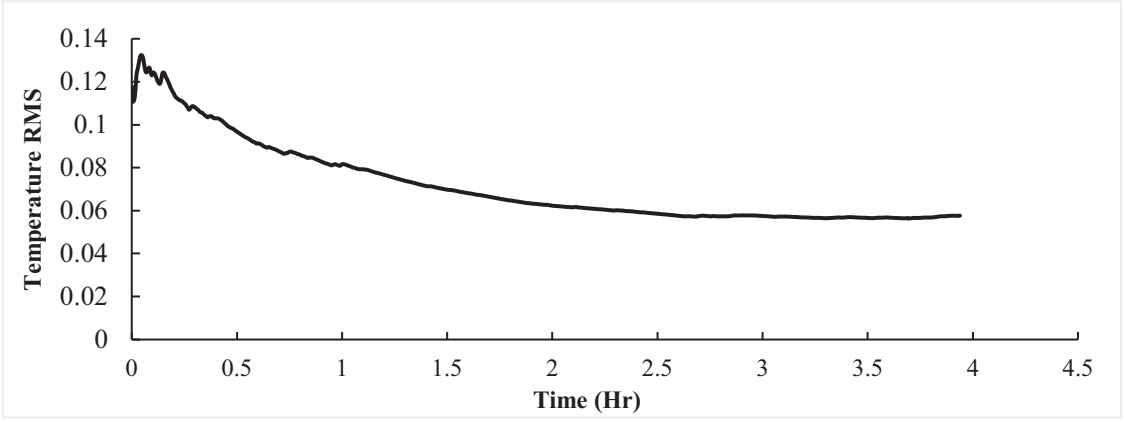

(b)

Fig. 3 – (a) Interior temperature (and running average) versus time, and (b) the temperature and running standard deviation (RMS) versus time.

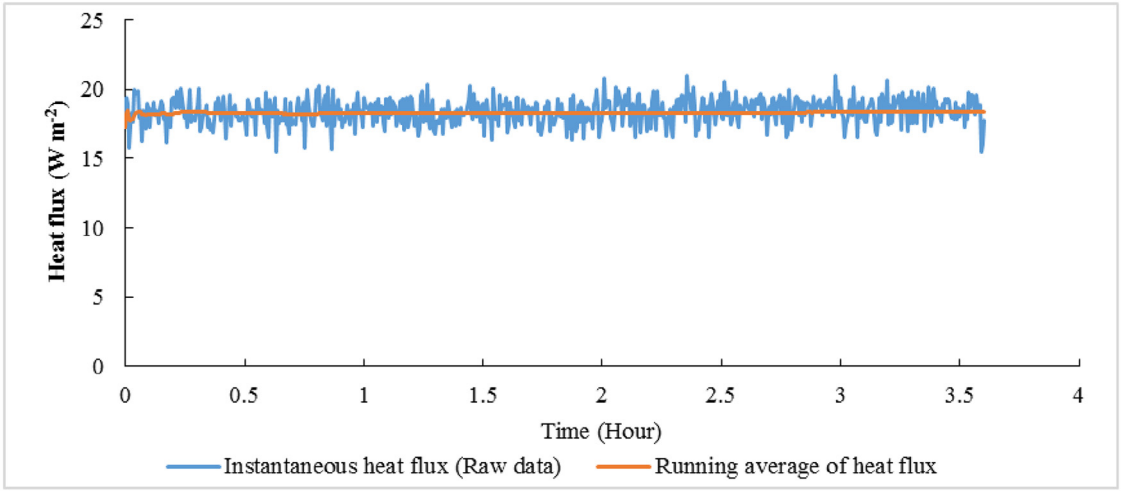

Fig. 4 – Instantaneous and running average heat flux sensor reading versus time.

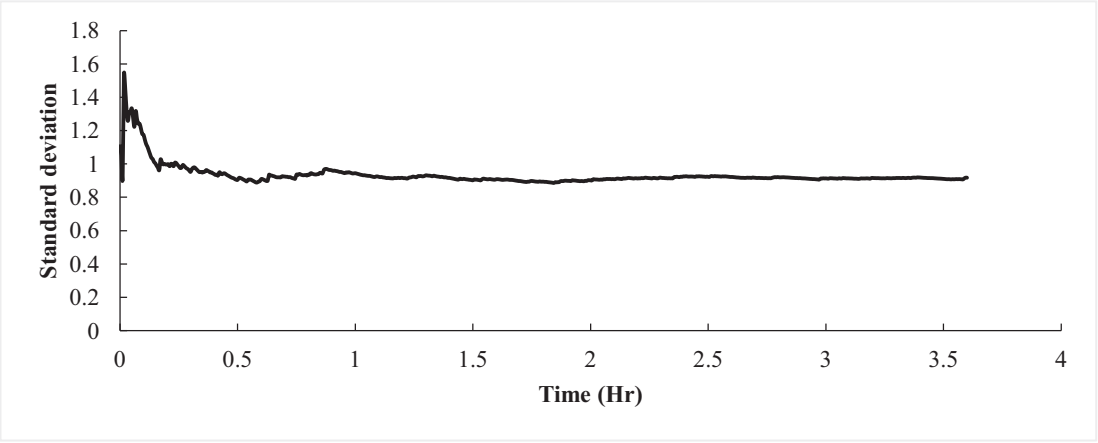

Fig. 5 – Running standard deviation heat flux sensor reading versus time.

Table 2 – Thermal properties of materials used in CFD.

Material	ρ_m (kg m^{-3})	C_m (J kg^{-1} K^{-1})	K_m (W m^{-1} K^{-1})
Cabinet insulation	1840	1450	0.0272
Refrigerator liner	1840	1225.1	0.3378
Refrigerator frame	7830	650	45.2
Magnet	8000	650	12.39
Gasket	1220	1600	0.15
Foam	1840	1450	0.022
Heater (copper)	8978	381	387.6
Air	1.225	1006.4	0.0242

et al., 2011; Sim and Ha, 2011). The air leakage through the gaps at the gasket region is also neglected (Yan et al., 2016).

3.1. *Boundary condition*

The ambient temperature was measured as 295 K and is assumed to remain constant approximately for the purposes of CFD. This temperature was the (measured) surface boundary temperature for all exposed insulated surfaces. However, there is a thermal boundary layer on the surface of the exposed gasket region. The boundary layer thickness was determined as approximately 5 mm based on experimental measurements with thermocouples. Therefore, the geometry simulated extends 5 mm into the air outside of the gasket region of the cabinet as shown in Fig. 8a. This thermal boundary layer of air is assumed as quiescent. All other outer surfaces are set as ambient temperature.

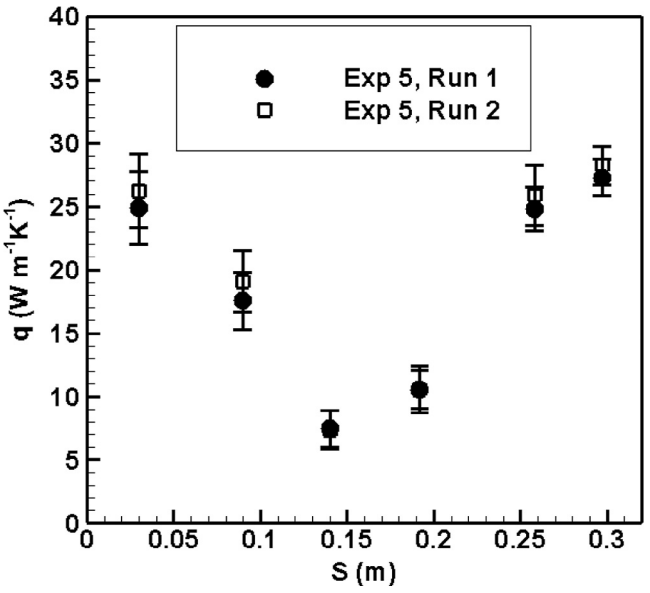

Fig. 6 – Measured surface heat flux (q) distribution versus the gasket surface path, S, for Experiment #5.

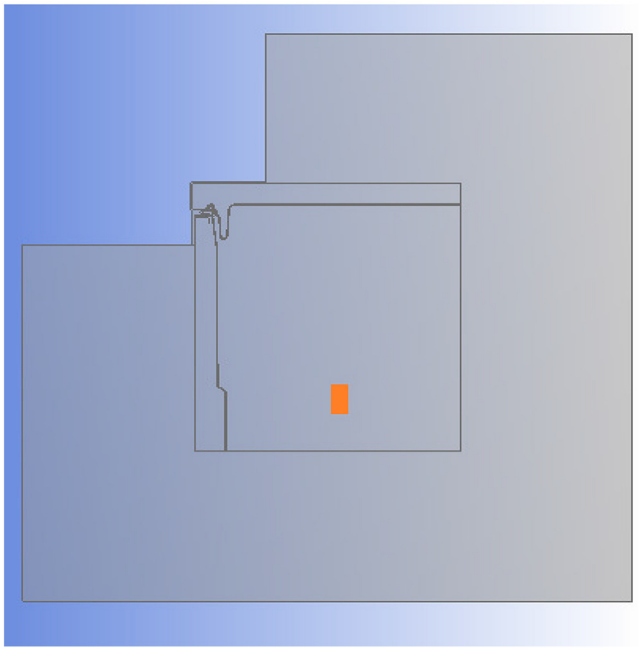

Fig. 7 – Two-dimensional geometry of the experimental test cabinet used in natural convection simulation; gravity vector points downward of the figure and shaded (orange) rectangular (10 cm × 5 cm) denotes the heater placed inside the compartment of the refrigerator. (For interpretation of the references to color in this figure legend, the reader is referred to the web version of this article.)

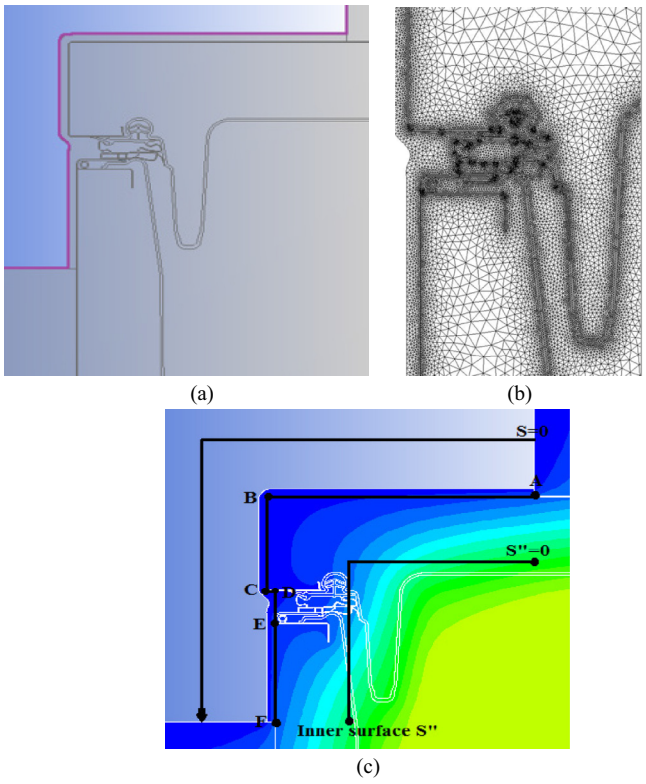

Fig. 8 – Zoom in of the (a) gasket region of the domain and specification of the boundary condition implemented in the CFD simulations with the purple line indicating the temperature of 298 K in the ambient environment, (b) corresponding mesh, a total of 380,800 finite volume cells are generated, and (c) two-dimensional gasket region showing different surface and interior path of heat flux (s and s″ are the coordinates along the outside and inner surfaces, respectively. Gravity direction is downward). (For interpretation of the references to color in this figure legend, the reader is referred to the web version of this article.)

Fig. 8b shows a mesh generated in the computational domain and the mesh is refined at the gasket region, and Fig. 8c presents the positions of the six flux sensors used in the experiment measurements with the coordinates along the surfaces.

3.2. *Convergence and mesh independent study*

Convergence of the CFD results to the "true" solutions is typically monitored by the residuals of the various equations being solved. However, commercial CFD packages such as ANSYS-FLUENT® have default residual criteria that are typically too large to ensure truly converged solutions. Therefore, the default values have all been reduced. The criteria for the energy equation have been reduced from its default of 0.001 to 10^{-12}. This value is rarely achieved. Therefore, to monitor whether a converged solution is achieved, the integral of heat flux on the wall is also monitored until it does not change with the further mesh refinement. For example, as shown in Fig. 9, the final result does not vary with further iteration steps and the final result does not change much when the cell number reaches 380,800. The y+ values of the first grid points should be less or equal to 1 when using enhanced wall functions, which was ensured to be met in the present simulation.

3.3. *Natural convection inside the refrigerator compartment*

In accordance of RHLM in the experimental setup, the heater is installed in the chamber of the refrigerator, which generates the airflow due to natural convection. When the heater is turned on, natural convective flow arises due to the change of the fluid density because of the temperature change. Boussinesq approximation, which is determined by the density change of the flow, is relatively small and the flow density is treated as a function of temperature (Oosthizen and Naylor, 1999)

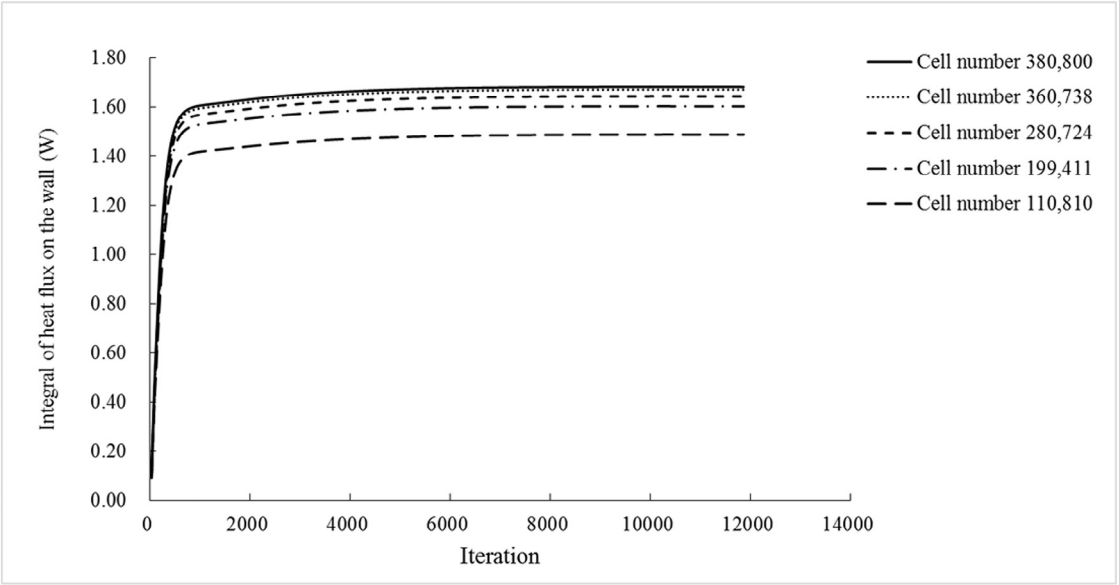

Fig. 9 – Monitor of mesh independent study.

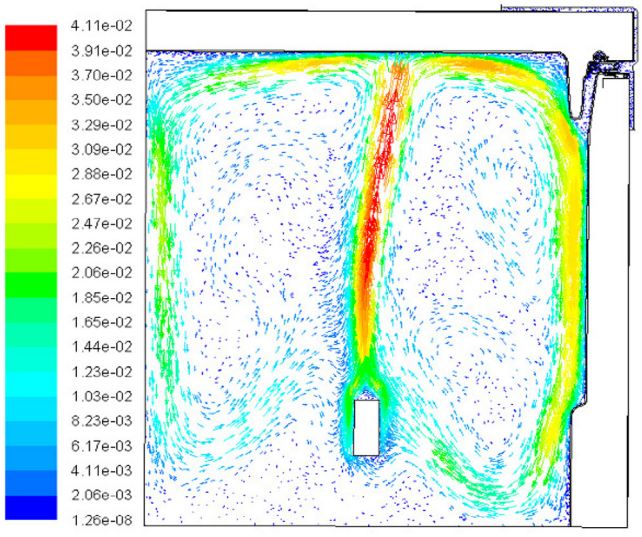

Fig. 10 – Zoom in of the velocity field of the air within the cabinet (with natural convection); gravity vector ($m\ s^{-1}$) points downward.

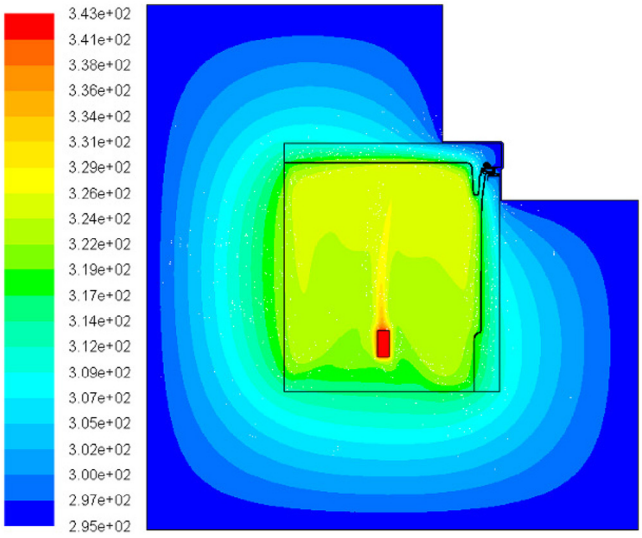

Fig. 11 – Contour of temperature (K) distribution of the cabinet (with natural convection); gravity vector points downward.

$$\rho - \rho_o = -\rho_o \beta (T - T_o) \tag{1}$$

where ρ is the flow density, and ρ_o is the operating density (which is 298 K in the present simulation). The range of the thermal expansion coefficient parameter is $10^{-4} < \beta < 10^{-3}$. The flow inside the refrigerator compartment is assumed as incompressible, and thus

$$\frac{\partial u_j}{\partial x_j} = 0 \tag{2}$$

By considering Equation (1), the momentum equation governing equation can be re-written as the following:

$$\rho\left(\frac{\partial u_i}{\partial t} + u_j \frac{\partial u_i}{\partial u_j}\right) = -\frac{\partial p}{\partial x_i} + \mu \Delta^2 u_i + \rho_o \beta (T - T_o) g + \rho_o g \tag{3}$$

All CFDs used to simulate the conditions of Experiments #1–5 purely use natural convection and the laminar flow model. Figs. 10 and 11 show the velocity and temperature within the chamber for a 9.2 W heat load with natural convection, respectively. Note that the velocity magnitudes are relatively small (on the order of ~0.01 m s^{-1}), which is indicative of near laminar flow conditions.

3.4. *Forced convection inside the freezer compartment*

We used CFD to study the effect of the freezer fan on the gasket region heat leakage. The turbulent model is applied to account for the turbulence flow generated due to the freezer fan and diffuser located within the cabinet. $k-\omega$ *SST* turbulence model with enhanced wall functions with y+ ≤ 1 for all surfaces was chosen as it uses a linear wall function and the boundary layer profile can be determined to predict the heat transfer between the wall and the fluid (Pulat et al., 2011; Verboven et al., 2000). All simulations use second order accurate discretization for all governing equations, and have iteratively adapted meshes to obtain grid independent solutions, as discussed above. The formulation of the *SST* model is shown in the following equations (Menter et al., 2003):

$$\frac{\partial(\rho k)}{\partial t} + \frac{\partial(\rho u_i k)}{\partial x_i} = p - \beta^* \rho k \omega + \frac{\partial}{\partial x_i}\left[\left(\mu + \sigma_k \mu_t\right)\frac{\partial k}{\partial x_i}\right] \tag{4}$$

$$\frac{\partial(\rho\omega)}{\partial t} + \frac{\partial(\rho u_i \omega)}{\partial x_i} = \alpha\rho S^2 + \frac{\partial}{\partial x_i}\left[\left(\mu + \sigma_\omega \mu_t\right)\frac{\partial \omega}{\partial x_i}\right] + 2(1-F)\rho\sigma'\frac{1}{\omega}\frac{\partial k}{\partial x_i}\frac{\partial w}{\partial x_i}\Bigg] \tag{5}$$

where F is the blending function. The term S is the invariant of strain rate $S_{ij} = \frac{1}{2}\left(\frac{\partial u_i}{\partial x_j} + \frac{\partial u_j}{\partial x_j}\right)$ and μ_t is the turbulence eddy diffusivity. The constants in the *SST* model are $\beta^* = 0.09$ and $\sigma' = 0.856$.

There is more than one way to estimate the initial turbulence inlet condition. For present purposes, the air flow into the electric fan is assumed as a fully developed internal pipe flow (before entering the fan). The initial turbulence kinetic energy, k_{int}, and specific dissipation rate, ω_{int}, are specified based on an assumed 5% turbulence intensity, I, at the diffuser

$$k_{\text{int}} = \frac{3}{2}\left(u_{\text{int},f} I\right)^2 \tag{6}$$

$$\omega_{\text{int}} = \frac{k_{\text{int}}^{\frac{1}{2}}}{Cu^{\frac{1}{4}} l} \tag{7}$$

in which Cu and l are the empirical constant and characteristic turbulence length scale (the fan diameter) to estimate the specific dissipation rate. The velocity of the cold air blowing from the electric fan, u_{ef}, is measured as the average of 1.0 m s^{-1},

Table 3 – Properties related to the electric fan installed in the freezer chamber.

Symbol	Cu	k_{int}	l	T_{ef}	u_{ef}	ω_{int}
Value	0.09	0.00404	0.1	258	1.0	16.59
Units	–	$m^2\ s^{-2}$	m	K	$m\ s^{-1}$	s^{-1}

and the temperature blowing out of the diffuser, T_{ef}, is 258 K (Table 3).

Temperature contours from a single forced convection simulation of the experiment under otherwise the same conditions as Experiment #1 are shown in Fig. 12. Corresponding surface heat flux profiles are shown in Fig. 13. By comparing the integrated heat leakage under the two curves in Fig. 13, the addition of the electric fan increases the heat leakage at the gasket surface by approximately 20%.

3.5. *Hot pipe modeling*

CFD was also chosen to model the effect of the hot pipe along the perimeter of freezer section gasket regions. The hot pipe, however, cannot simply be added to the above described simulations of the experimental test cabinet under forced convection conditions directly. This would be inconsistent with RHLM (adding a hot pipe on the cold external surface). Therefore, the $k-\omega$ *SST* simulation described above was modified to have a real freezer temperature of 258 K (inlet temperature for the freezer fan), an ambient temperature of 295 K, and a hot pipe temperature of static air at 313 K. In addition, the path surface, *s*, defined in Fig. 8c, can no longer be used to calculate the energy leakage rate. This is because the hot pipe is a new source of thermal energy, thus some of the energy flows into the cabinet (the portion of interest), but much flows out of the cabinet. This latter portion obscures the desired calculation of the energy leakage into the cabinet for path *s* since local to the hot pipe along path *s* the heat flow is actually outward. This would seem to produce a net decrease in the heat leakage.

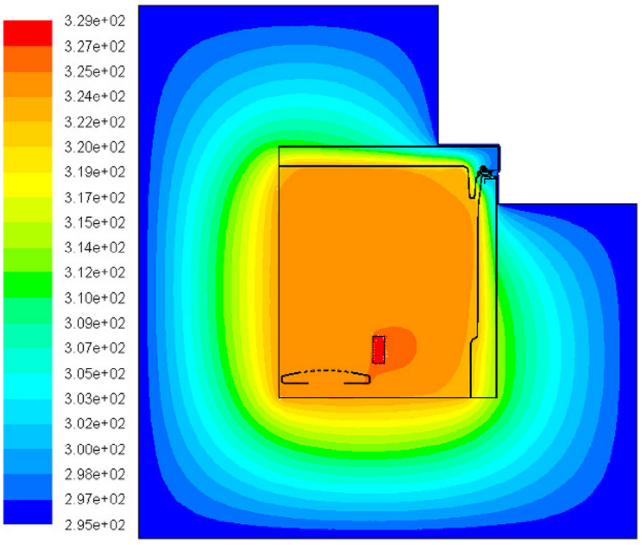

Fig. 12 – Temperature (K) contours for a CFD simulation with the freezer electric fan and diffuser.

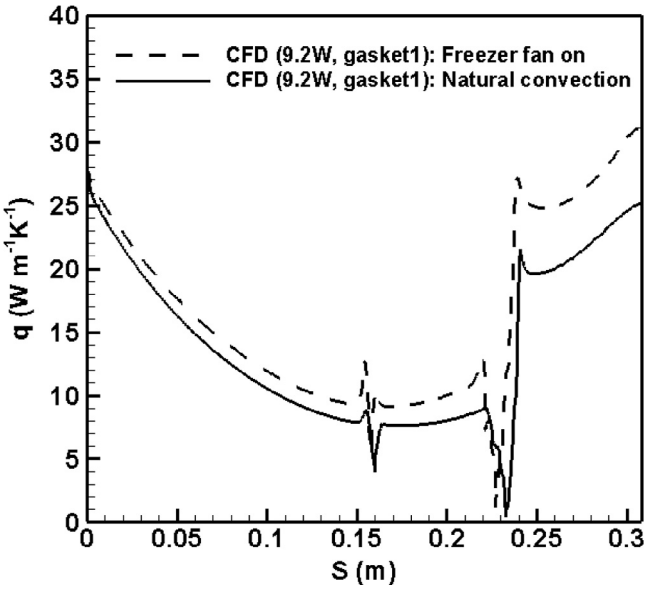

Fig. 13 – Comparison of the surface heat flux (*q*) along the outside surface of the gasket surface (*s*) from CFD of the cabinet with 9.2 W heat load showing the effects of adding a freezer fan inside the box. The integrated increase in heat transfer is 20% due to forced convection.

We therefore examined inner surface path *s″* from Fig. 8c. By placing the path interior to the hot pipe only the contribution of the heat leakage into the cabinet is recovered, as shown in Fig. 14 (note that the heat flows are now negative due to the cold freezer conditions in the cabinet).

The "jaggedness" of the curves is due to the fact that the paths *s″* cross through various materials such as very thin cross sections of the cabinet liner and/or metal surfaces. These materials have much larger thermal conductivities than the insulation (see

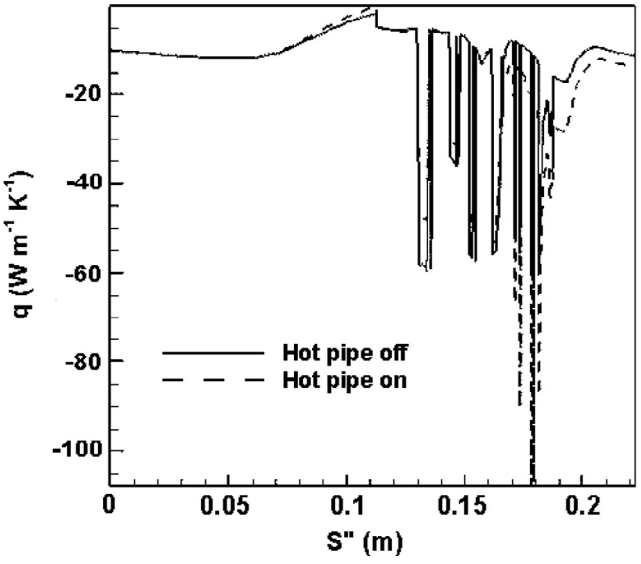

Fig. 14 – Surface heat flux measured along the inner gasket surface *s″* for freezer temperature conditions with the freezer fan on and the hot pipe both off and on.

Table 2). The heat flow therefore finds these (relatively thin) paths to travel through around the foam insulation. The curves shown in Fig. 14 can nevertheless be integrated and then divided by the temperature difference to get the respective heat leakage values of –0.078 W m^{-1} K^{-1} and –0.086 W m^{-1} K^{-1} for the conditions of the hot pipe on and off, respectively. These are smaller than the values discussed previously for two reasons. Firstly, the path length is shorter so the heat leakage in the unit of W m^{-1} obtained by integrating is somewhat smaller. Secondly, and related, is that there is some heat flow tangentially along either edge that gets neglected using these path lines. However, the only thing that is truly important is the ratio, which is approximately 10%. Therefore, as determined above, the freezer fan will increase heat leakage values by as much as 20% alone, whereas if the hot pipe is also active the heat leakage is increased by an additional 10%.

4. Combined experimental and computational methodology

Fig. 15a shows all of the raw data produced by the experiments and the CFD of the experimental test cabinet. As noted above, the effects of the freezer fan and the hot pipe were studied purely with CFD. The CFD is two-dimensional and is not expected to produce the same temperature difference as the three-dimensional experimental test cabinet (in the CFD the heating element is infinitely long in the third direction). Nevertheless, the "shape" of the surface heat flux is expected to be the same in the two-dimensional CFD in comparison to the centerline (symmetry plane) of the experimental test cabinet surface. Therefore, the CFD is only used to produce the shape factors necessary to fill in the information between the six experimental heat flux sensors. What needs to be determined is the multiplication factor needed to correct the CFD produced shape factors to "best fit" the experimental data. Note that for a given gasket any of the CFD profiles produced at the various heat loads can be used as the profiles are independent of temperature difference when normalized. The "best fit" is defined for present purposes as that scaling factor which minimizes the mean square error – the so called Least Mean Square Error (LMSE) approach. The mean square error is defined as

$$MSE = \sum_{n=1}^{6} (Exp_n - \alpha f_n)^2 \tag{8}$$

where Exp_i denotes the individual heat flux sensor measurements (i.e., $s = 0.03$ m, 0.09 m, 0.14 m, 0.192 m, 0.258 m, and 0.303 m) (Fig. 8c, A–F). The term f_n denotes the corresponding point measurement obtained from CFD simulation. Once obtained the entire CFD curve for that experiment is multiplied by the correction factor α and the experimental data and corrected CFD profile can be plotted and/or analyzed. The final CFD profile is then numerically integrated over the entire domain length for the path s of Fig. 8c. This yields the heat leakage rate in watts per unit length of the gasket region, which is written as W m^{-1}. Finally, the W m^{-1} values are then divided by the experimentally measured temperature difference to produce the final heat leakage values in the unit of W m^{-1} K^{-1}.

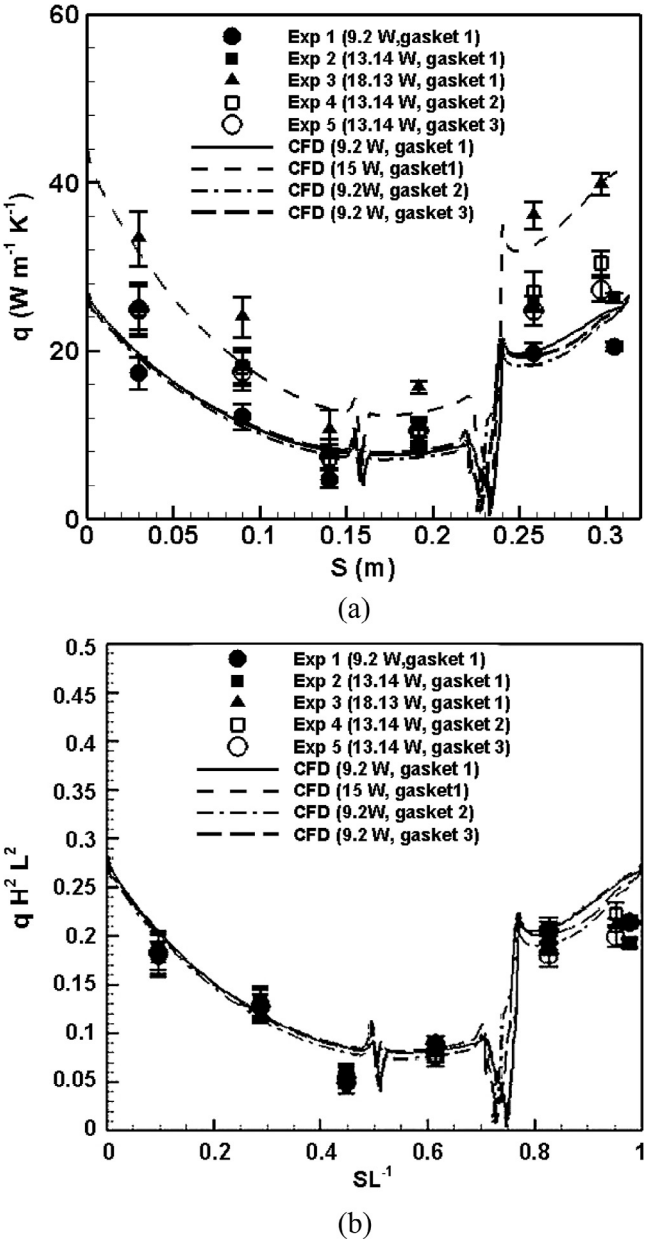

Fig. 15 – Experimental and CFD obtained surface heat fluxes as a function of the surface path coordinate: (a) the original raw data, and (b) the same data non-dimensionalized by the gasket surface length (*L*) and the heat load (*H*) in Watts. The "error" bars are the standard deviation of the data used to calculate the average heat fluxes.

By using LMSE method, the averaged effective heat leakage is calculated as 0.2 W m^{-1} K^{-1} for the sample domestic refrigerator.

As shown in Fig. 15a, the experimental point measurements lie near to the CFD curve, which indicates reasonable agreements between CFD and the experiment. The reasons explaining the discrepancy between experimental and CFD results are possibly in the two major aspects: (1) The CFD is two dimensional based while the flow is three-dimensional in reality. By being two dimensional, the depth of the computational domain is considered as infinite, which is different from reality.

(2) Although the test cell is well-insulated to the best of our effort, it is inevitable that heat leaks at the corners of the test cell, which may contribute to the inaccuracy of experimental measurement as whether heat leakage at the corners of the test cell is linear to temperature difference is not known for sure.

5. Conclusion

In this paper, we presented the experimental method based on RHLM and CFD simulation to investigate the heat leakage at the door gasket region of both the refrigerator and freezer. The CFD simulation has modeled the flow field and temperature field to inside the refrigerator and freezer cabinets to capture the near-wall heat transfer at the door gasket region. The operation of the electric fan is estimated to increase the heat leakage by 20% based on CFD results, whereas the hot pipe along the perimeter of freezer section gasket regions contributes to an additional 10% of the heat leakage if in operation. We proposed a method to combine the experimental and CFD to provide a continuous heat flux curve to fill up the missing data between experimental measurement points by using LSME, in which way, the averaged effective heat leakage (h) at the door gasket is estimated as 0.20 W m^{-1} K^{-1}. The total heat loss at the gasket and its corresponding percentage accounted for the total energy of the refrigerator is summarized in Table 4, where ΔT indicates the absolute temperature difference between the ambient environment and the fresh food/freezer compartment, Q is the total heat leakage at the gasket region, including the consideration of the length of the gasket region (l_g). The pressure term P_{cmp} is the power of the compressor of the sample domestic refrigerator, which is measured as 95 W. The term η indicates the percentage of the heat leakage at the gasket region accounted for from the total energy.

$$Q = h * l_g * \Delta T \tag{9}$$

$$\eta = \frac{Q}{P_{cmp}} * 100\% \tag{10}$$

Table 4 – The summarized total heat loss due to the gasket region based on the dimensions of the sample refrigerator.

Variable	h (W m^{-1} K^{-1})	l_g (m)	ΔT (K)	Q (W)	P_{cmp} (W)	η (%)
Fresh food	0.20	3.4	20	13.6	95	14
Freezer	0.20	2.4	35	16.8	95	17

Appendix: Experimental measured heat flux values

Table A1 – Measured average and root mean square (rms) of heat flux in Experiments #1–#5.

Experiment #	1		2		3		4		5	
Gasket	Original		Original		Original		Black		White	
P_{rhl} (W)	9.20		13.14		18.13		13.14		13.14	
ΔT (K)	20.2		26.6		34.6		25.2		25.6	
Sensor # (W m^{-2})	$\bar{q}$	$\bar{q}_{rms}$	$\bar{q}$	$\bar{q}_{rms}$	$\bar{q}$	$\bar{q}_{rms}$	$\bar{q}$	$\bar{q}_{rms}$	$\bar{q}$	$\bar{q}_{rms}$
A	17.3	25.2	33.4	3.23	2.58	1.94	24.86	3.20	24.9	2.88
B	12.2	18.3	24.0	2.43	2.04	1.55	18.06	2.15	17.6	2.28
C	4.76	7.79	10.6	2.35	1.72	1.06	7.13	1.24	7.46	1.45
D	8.57	11.2	15.7	0.76	0.59	0.71	10.65	0.93	10.5	1.52
E	19.7	25.7	36.1	1.61	0.78	1.31	27.02	2.39	24.8	1.69
F	20.5	26.3	39.9	1.31	0.60	0.6	30.46	1.51	27.3	1.43

REFERENCES

Bansal, P., Vineyard, E., Abdelaziz, O., 2011. Advances in household appliances – a review. Appl. Therm. Eng. 31, 3748–3760.

Boughton, B.E., Clausing, A.M., Newell, T.A., 1996. An investigation of household refrigerator cabinet thermal loads. HVAC&R Res. 2, 135–147.

Brent, T.G., Dariush, K.A., Daniel, T., 1995. Energy efficiency improvements for refrigerator/freezers using prototype doors containing gas-filled panel insulating systems. In: Proceedings of the 46th International Appliance Technical. Urbana, IL.

Conceição António, C., Afonso, C.F., 2011. Air temperature fields inside refrigeration cabins: a comparison of results from CFD and ANN modelling. Appl. Therm. Eng. 31, 1244–1251.

Flynn, S., Rouch, K., Fine, H.A., 1992. Finite Element Analysis of Heat Transfer Through the Gasket Region of Refrigerator/Freezer. United States Environmental Protection Agency, Office of Air and Radiation.

Fukuyo, K., Tanaami, T., Ashida, H., 2003. Thermal uniformity and rapid cooling inside refrigerators. Int. J. Refrigeration 26, 249–255.

Ghassemi, M., Shapiro, H., 1991. Review of energy efficiency of refrigerator/freezer gaskets, U.S. EPA, Air and Energy Engineering Research Laboratory.

Gupta, J.K., Ram Gopal, M., Chakraborty, S., 2007. Modeling of a domestic frost-free refrigerator. Int. J. Refrigeration 30, 311–322.

Hasanuzzaman, M., Saidur, R., Masjuki, H.H., 2009. Effects of operating variables on heat transfer and energy consumption of a household refrigerator-freezer during closed door operation. Energy 34, 196–198.

Hessami, M.-A., Hilligweg, A., 2003. Energy efficient refrigerators: the effect of door gasket and wall insulation on heat transfer. In: ASME 2003 International Mechanical Engineering Congress and Exposition, Heat Transfer, Volume 3. Washington, DC, USA, pp. 57–64.

Huelsz, G., Gómez, F., Piñeirua, M., Rojas, J., de Alba, M., Guerra, V., 2011. Evaluation of refrigerator/freezer gaskets thermal loads. HVAC&R Res 17, 133–143.

Kumlutaş, D., Karadeniz, Z.H., Avcı, H., Özşen, M., 2012. Investigation of design parameters of a domestic refrigerator by artificial neural networks and numerical simulations. Int. J. Refrigeration 35, 1678–1689.

Laguerre, O., Ben Amara, S., Flick, D., 2005. Experimental study of heat transfer by natural convection in a closed cavity: application in a domestic refrigerator. J. Food Eng. 70, 523–537.

Laguerre, O., Ben Amara, S., Moureh, J., Flick, D., 2007. Numerical simulation of air flow and heat transfer in domestic refrigerators. J. Food Eng. 81, 144–156.

Menter, F.R., Kuntz, M., Langtry, R., 2003. Ten years of industrial experience with the SST turbulent model. In: Turbulence, Heat and Mass Transfer 4: Proceedings of the Fourth International Symposium on Turbulence, Heat and Mass Transfer. Begell House, Inc., Antalya, Turkey.

Mohanraj, M., Jayaraj, S., Muraleedharan, C., 2012. Applications of artificial neural networks for refrigeration, air-conditioning and heat pump systems – a review. Renew. Sustain. Energy Rev. 16, 1340–1358.

Mohanraj, M., Jayaraj, S., Muraleedharan, C., 2015. Applications of artificial neural networks for thermal analysis of heat exchangers – a review. Int. J. Therm. Sci. 90, 150–172.

Oosthizen, P., Naylor, D., 1999. Introduction to Convective Heat Transfer Analysis. McGraw-Hill Science/Engineering/Math, New York.

Pulat, E., Isman, M.K., Etemoglu, A.B., Can, M., 2011. Effect of turbulence models and near-wall modeling approaches on numerical results in impingement heat transfer. Numer. Heat Transf. B Fundament. 60, 486–519.

Sim, J.S., Ha, J.S., 2011. Experimental study of heat transfer characteristics for a refrigerator by using reverse heat loss method. Int. Commun. Heat Mass Transf. 38, 572–576.

Tao, W.-H., Sun, J.-Y., 2001. Simulation and experimental study on the air flow and heat loads of different refrigerator cabinet designs. Chem. Eng. Commun. 186, 171–182.

Verboven, P., Scheerlinck, N., Baerdemaeker, J.D., Nicolaï, B.M., 2000. Computational fluid dynamics modelling and validation of the isothermal airflow in a forced convection oven. J. Food Eng. 43, 41–53.

Xie, G., Bansal, P.K., 2000. Analysis of defrosted water evaporation from three water trays in refrigerators. Appl. Therm. Eng. 20, 651–669.

Yan, G., Chen, Q., Sun, Z., 2016. Numerical and experimental study on heat transfer characteristic and thermal load of the freezer gasket in frost-free refrigerators. Int. J. Refrigeration 63, 25–36.